



City Research Online

City, University of London Institutional Repository

Citation: Stefanitsis, D., Malgarinos, I., Strotos, G., Nikolopoulos, N., Kakaras, E. & Gavaises, M. (2017). Numerical investigation of the aerodynamic breakup of Diesel and heavy fuel oil droplets. *International Journal of Heat and Fluid Flow*, 68, pp. 203-215. doi: 10.1016/j.ijheatfluidflow.2017.10.012

This is the accepted version of the paper.

This version of the publication may differ from the final published version.

Permanent repository link: <https://openaccess.city.ac.uk/id/eprint/19883/>

Link to published version: <https://doi.org/10.1016/j.ijheatfluidflow.2017.10.012>

Copyright: City Research Online aims to make research outputs of City, University of London available to a wider audience. Copyright and Moral Rights remain with the author(s) and/or copyright holders. URLs from City Research Online may be freely distributed and linked to.

Reuse: Copies of full items can be used for personal research or study, educational, or not-for-profit purposes without prior permission or charge. Provided that the authors, title and full bibliographic details are credited, a hyperlink and/or URL is given for the original metadata page and the content is not changed in any way.

City Research Online:

<http://openaccess.city.ac.uk/>

publications@city.ac.uk

Numerical investigation of the aerodynamic breakup of Diesel and heavy fuel oil droplets

Keywords

Droplet breakup; Diesel; HFO; VOF; representative engine conditions.

Nomenclature

Roman symbols

| | |
|------------|--|
| A | Area [m ²] |
| C_d | Drag coefficient [-] |
| D | Droplet diameter [m] |
| f | Vortex shedding frequency [Hz] |
| g | Gravitational acceleration [m/s ²] |
| L | Distance [m] |
| m | Mass [kg] |
| N | Viscosity ratio [-] |
| Oh | Ohnesorge number [-] |
| P | Pressure [Pa] |
| Re | Reynolds number [-] |
| S | Surface [m ²] |
| St | Strouhal number [-] |
| T | Temperature [K] |
| t_{init} | Breakup initiation time [s] |
| t_{sh} | Shear breakup timescale [s] |
| t | Time [s] |
| U | Velocity [m/s] |

We Weber Number [-]

Greek symbols

| | |
|---------------|------------------------------|
| α | Volume fraction [-] |
| ε | Density ratio [-] |
| μ | Dynamic viscosity [kg/(s·m)] |
| ρ | Density [kg/m ³] |
| σ | Surface tension [N/m] |

Subscripts

| | |
|--------|--------------|
| O | Initial |
| cr | Cross-stream |
| $crit$ | Critical |
| d | Droplet |
| f | Frontal |
| g | Gas phase |
| l | Liquid phase |
| m | Mean |
| rel | Relative |
| str | Streamwise |

1 Introduction

Secondary atomization plays an important role in the operation of liquid injection systems encountered in many engineering applications such as in oil burners and internal combustion engines. During secondary atomization, fuel droplets experience large deformation and subsequent breakup due to the exertion of aerodynamic forces on them. The relative velocity between the liquid droplet and the surrounding gas is responsible for the aerodynamic forces that tend to deform the droplet, while fluid properties such as viscosity and surface tension induce forces that resist deformation. The most important non-dimensional numbers controlling the aerodynamic droplet breakup are the

Weber (We), the Ohnesorge (Oh) and the Reynolds (Re) numbers as well as the density (ε) and viscosity (N) ratios of the two phases [1]:

$$We = \frac{\rho_g U_{rel,0}^2 D_0}{\sigma} \quad Oh = \frac{\mu_l}{\sqrt{\rho_l \sigma D_0}} \quad Re = \frac{\rho_g U_{rel,0} D_0}{\mu_g} \quad \varepsilon = \frac{\rho_l}{\rho_g} \quad N = \frac{\mu_l}{\mu_g} \quad (1)$$

As breakup process is not instantaneous, the breakup timescale proposed by Nicholls and Ranger [2] can be used as a convenient non-dimensionalisation parameter for understanding the temporal development of the process:

$$t_{sh} = \frac{D_0}{U_{rel,0}} \sqrt{\varepsilon} \quad (2)$$

It is generally considered [1] that when the Oh number is less than 0.1 the droplet breakup is mostly influenced by the We number. Apart from the vibrational mode ($We < 11$), four major breakup regimes are encountered based on the We number. The first breakup mode is called bag breakup ($11 < We < 35$) owing its name to the bag resembling shape that the drop takes during its deformation. As the We number is further increased up to 80, the multimode breakup regime is encountered, which is an intermediate stage between the bag and sheet-thinning breakup modes. In this regime different drop shapes are encountered with the most dominant being the bag-stamen, the dual bag and the plume/shear. During the sheet-thinning breakup mode ($80 < We < 350$) a liquid sheet is formed at the droplet periphery which initially breaks into ligaments and eventually into small fragments. The final breakup mode ($We > 350$) is called catastrophic and is attributed to drop instabilities such as Rayleigh-Taylor (R-T) and Kelvin-Helmholtz (K-H). These instabilities create unstable waves on the leading surface of the drop, which grow in time and eventually lead to the breakup of the droplet.

The test liquids used in the majority of the existing experimental studies are water and ethanol and only a few experimental works have examined actual fuels such as Diesel oil, which is a widely used

liquid in internal combustion engines and is also a focus of the current study. Arcoumanis et al. [3], were one of the first who studied experimentally the breakup of Diesel droplets using the continuous air jet arrangement. They examined We numbers ranging from 14 up to 10000 and produced graphs of the breakup time as function of the We number and droplet diameter. In addition, they provided photographs of the breakup process and reported three breakup modes: a) bag, b) sheet-thinning and c) catastrophic. For the same breakup regimes, a series of works related to Diesel fuel were reported by the group of R. D. Reitz [4-6], examining a wide range of We numbers (56-532), Re numbers (509-8088), and density ratios (79-700); in all cases, the Oh number was kept below 0.065. They measured the droplet deformation along its trajectory accompanied with photographs of the breakup process. They concluded that for the examined conditions, the Re number does not affect the breakup process but rather the We number is the controlling parameter; this conclusion has proved that the sheet-thinning breakup regime (formerly known as shear stripping) is not ought to viscous stresses but rather to aerodynamic forces. Another group that employed Diesel fuel for their experimental work is that of C. S. Lee [7, 8]. In their experimental setup they ejected with a droplet generator (nozzle and vibrating piezo stack) mono-dispersed droplets into a gas stream. They investigated the microscopic (droplet scale) and macroscopic (spray scale) breakup characteristics in three breakup regimes (vibrational, bag and sheet-thinning) for We numbers in the range of 4.3 up to 383. They generated images of the single droplet breakup process and presented graphs of the temporal evolution of droplet mean velocity and spatial evolution of droplet mean diameter.

The aforementioned experimental works were mainly focused on low viscosity liquids, resulting in low Oh numbers. Regarding the experimental studies with large Oh numbers, high viscous liquids were employed such as silicon oil and glycerol aquarium solutions. Hinze [9] investigated the breakup of gas oil droplets exposed to an air stream for We numbers in the range of 13 up to 40 and Oh from 0.01 up to 2. They concluded that the rate of droplet deformation decreases with increasing Oh , while for $Oh > 2$ no breakup occurs for the examined conditions. Hanson et al. [10] examined the aerodynamic breakup of water, methyl-alcohol and silicon oil droplets for We numbers in the range of 3.6 up to 23.8 and Re

numbers ranging from 317 up to 946. They observed that the air shock wave itself is not the cause of breakup, but rather the air flow stream induced behind it, whilst also found that for $\mu_L > 10 \text{ mPa}$ the liquid viscosity affects the critical breakup velocity (minimum velocity required for breakup). Gel'fand et al. [11] used the shock tube technique to study the breakup of water and glycerine droplets for We numbers from 5 up to 25. They proposed empirical correlations for the minimum We number required for breakup, the breakup initiation time and the total breakup time as a function of the Laplace number ($La = 1/Oh^2$). Hsiang and Faeth [12-14] used the shock tube method as well and studied the breakup of various liquids in a broad range of We (0.5-600), Oh (<560), Re (>300) and ϵ (>580) numbers. They combined their results with previous studies to construct an $Oh-We$ map where the various breakup regimes are presented. Furthermore, they concluded that for $Oh > 1$ the critical We number for the onset of breakup is roughly proportional to Oh , while for $Oh > 0.1$ the breakup time for the examined conditions increases with the Oh number. Zhao and co-workers published a series of works [15-17] using the continuous air jet arrangement to investigate the bag and bag-stamen breakup of water, ethanol and glycerol droplets in We numbers from 9.4 up to 49 and Oh numbers from 0.0018 up to 0.36. They developed a theoretical model based on the Rayleigh-Taylor instability and proposed a correlation for the prediction of the critical We number as function of Oh number. In addition, they found that the maximum droplet deformation decreases with increasing Oh number, while the mean diameter of the fragments increases. Finally, it should be mentioned that there are no experimental data for HFO droplets which is also a focus of this study.

With regards to numerical modelling of breakup, there are no studies that employ HFO or Diesel as test liquids; instead, there are some works investigating non-dimensional numbers that resemble viscous fluids (large Oh numbers) and Diesel engine conditions (small density ratios), but without referring to specific fluids and the exact combination of non-dimensional parameters associated with actual engine conditions. Han and Tryggvason [18] studied the breakup of impulsively accelerated drops using a finite difference/front tracking numerical technique in a 2D axisymmetric domain. They investigated Oh numbers up to 15.8 and found that for the examined conditions the increase of Oh

number leads to the decrease of the rate of deformation and the alternation of the droplet shape from forward-facing bag to oblate. Aalburg [19] used the Level Set (LS) interface tracking method to study the deformation (but no breakup) of droplets at small Re numbers (25-200) and density ratios (2-32), while the Oh number ranged from 0.001 up to 100. He found that by decreasing the density ratio below 32, the critical We number for breakup increases, while for density ratios greater than 32 the breakup outcome is independent of the density ratio. Quan and Schmidt [20] used a finite volume staggered mesh method to examine the drag force and deformation of impulsively accelerated drops. They tested two Oh numbers (1.12 and 2.24) for a small range of We numbers (0.4-40) and density ratios (10-50) and observed that the increase of Oh number results in smaller deformation and drag coefficient. Wadhwa et al. [21] employed a hybrid compressible-incompressible numerical method (liquid is modelled as incompressible while gas is modelled as compressible) to study the deformation and drag of decelerating drops injected in a quiescent gas and found that they both increase with decreasing Oh number. Jing and Xu [22] simulated the deformation and breakup of liquid drops in a gas flow using the Level Set method in a 2D axisymmetric domain. They examined We numbers from 2.7 up to 275, Oh numbers from 0.0008 up to 0.831 and ε from 10 up to 100, and concluded that the increase of Oh number for the examined conditions can result in no breakup. Kekesi et al. [23] used a 3D VOF method to study the breakup of liquid drops in small We (0.1-20), Re (20-200) and ε numbers (20-80), while the Oh numbers ranged from 0.007 up to 1. They identified 5 new breakup modes (jellyfish shear, thick rim shear, thick rim bag, rim shear and mixed) in the bag breakup regime and also developed a new breakup map in the $Re-N/\sqrt{\varepsilon}$ plane where the different breakup regimes were presented irrespectively of the We number. Yang et al. [24, 25] used a coupled LS-VOF method in a 3D domain to simulate the aerodynamic droplet breakup in the bag and multimode breakup regimes ($We=8-70$, $Oh=0.001-2$ and $\varepsilon=800$) as well as the sheet-thinning regime ($We=225$, $Oh<0.015$ and $\varepsilon<200$). They developed a theoretical model based on the R-T instability for predicting the critical We number and also found that the drag coefficient and the drop deformation are affected by the density ratio even when it exceeds the value of 32, as opposed to the findings of Aalburg [19]. Shao et al. [26]

used the 3D-LS method to investigate the unsteady drag coefficients of deforming liquid drops with We numbers from 1 up to 10, Oh numbers from 0.0007 up to 0.1 and density ratios from 6.25 up to 40. They found that the unsteady drag coefficient is influenced mostly by the density ratio, while the change in Oh number has a small effect.

To the best of our knowledge, the current study is the first numerical work that investigates the aerodynamic breakup of HFO droplets under representative conditions for Diesel engines (We , Oh , Re , and ϵ). However, the droplet evaporation and heating are not taken into account as they will be investigated in future research; an indication about their significance on the process is presented in Appendix A using a 0D model. The examined non-dimensional parameters are presented in **Figure 1** along with those of the aforementioned numerical studies depicted on the $Oh-We$ and $Re-N/\sqrt{\epsilon}$ planes; both planes are required for the complete description of the physical parameters. The representative conditions for engines fueled with light Diesel and HFO are presented on the same figure as well; more details regarding the determination of the engine conditions can be found in section 2. Although some previous numerical studies have examined We and Oh numbers corresponding to conditions of engines fueled with HFO, there are no studies matching exactly the set of the non-dimensional numbers (We , Oh , Re and ϵ) required to characterize the full range of conditions realised; the present work aims to fill this gap in knowledge.

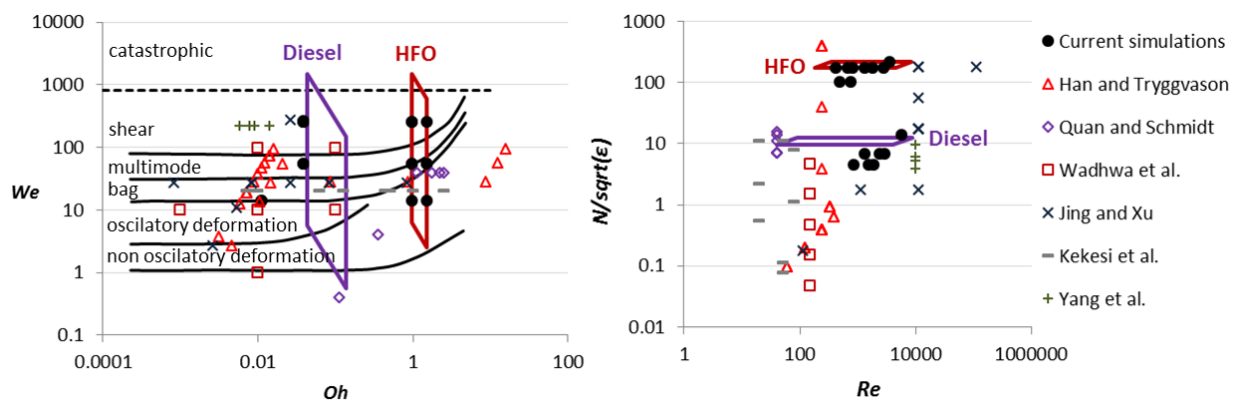


Figure 1. Examined parameters of current and previous numerical studies presented in a) the $Oh-We$ plane and b) the $Re-N/\sqrt{\epsilon}$ plane.

In the following sections initially the computational setup and the cases examined are presented, followed by the model validation against published experimental data for Diesel fuel. Subsequently, a parametric study is performed for the Oh number and the density ratio and their effect on the breakup mode and on various parameters such as the droplet deformation, surface area, drag coefficient and breakup initiation time is discussed. Finally, the most important conclusions are summarized in the last section.

2 Computational setup and examined cases

The numerical model solves the Navier-Stokes equations coupled with the Volume of Fluid (VOF) methodology of Hirt and Nichols (1981) [27] for capturing the interface between liquid and gas. The surface tension forces are included in the momentum equation by using the Continuum Surface Stress (CSS) model by Lafaurie et al. (1994) [28]. The CFD simulations are carried out using the commercial CFD tool ANSYS FLUENT v16 [29] with the inclusion of various user defined functions (UDFs), used for the integration of the adaptive local grid refinement technique [30] and the adaptive time-step scheme for the implicit VOF solver. The CFD model has been developed and validated in previous works for numerous applications including the free fall of a droplet in Malgarinos et al (2015) [30], the droplet impingement on a flat wall in Malgarinos et al. (2014) [31], the collision of droplet with particle in Malgarinos et al. [32-34], the aerodynamic droplet breakup in conditions of high density ratios in Strotos et al (2015, 2016) [35-38] and the static droplet evaporation in Strotos et al. (2016) [37-39]. In the present study the model validation is extended to the cases of Diesel fuel droplets and the model results are compared against the experimental data of Arcoumanis et al. [3], Liu and Reitz [4] and Lee and Reitz [5]; the latter work is additionally referring to high pressure conditions which resemble those exhibited in Diesel engines

The computational domains and boundary conditions are presented in Figure 2 for the 2D axisymmetric approach as well as the 3D approach (the plane corresponding to the 2D simulation is

also shown). The 3D approach (in relevance to the 2D one) apart from being able to capture the 3D flow structures, is also able to capture the droplet motion and deformation along the cross-stream direction (X-axis in the 3D domain). This secondary motion is only present in the experiments of Liu and Reitz [4] and Lee and Reitz [5] and its significance is discussed in a subsequent section. In order to decrease the computational cost only the half of the droplet is simulated, applying symmetry boundary conditions similar to [36]. The grid comprises of rectangular/hexahedron cells; the base grid resolution is 3 cells per radius (cpR) and 6 levels of refinement (or 5 for the 3D case) are sequentially applied in order to achieve the desired resolution of 192cpR (or 96cpR). Systematic runs with 48, 96, 192 and 384cpR have shown that the resolution of 96cpR is adequate as the mean drop velocity and deformation change less than 1% when a finer grid is used. In Figure 2c the levels of refinement are shown around the liquid-gas interface. The refinement algorithm identifies the cells of the interface (those with a VOF isovalue of 0.5) and then calculates the distance of all computational cells from the interface. Starting with the first refinement level (or the last for coarsening) and continuing with the rest, the cells are refined/coarsened based on the aforementioned distance and the desired thickness of each refinement level. This procedure is performed every 10-20 timesteps so as the interface lies always in the densest grid region.

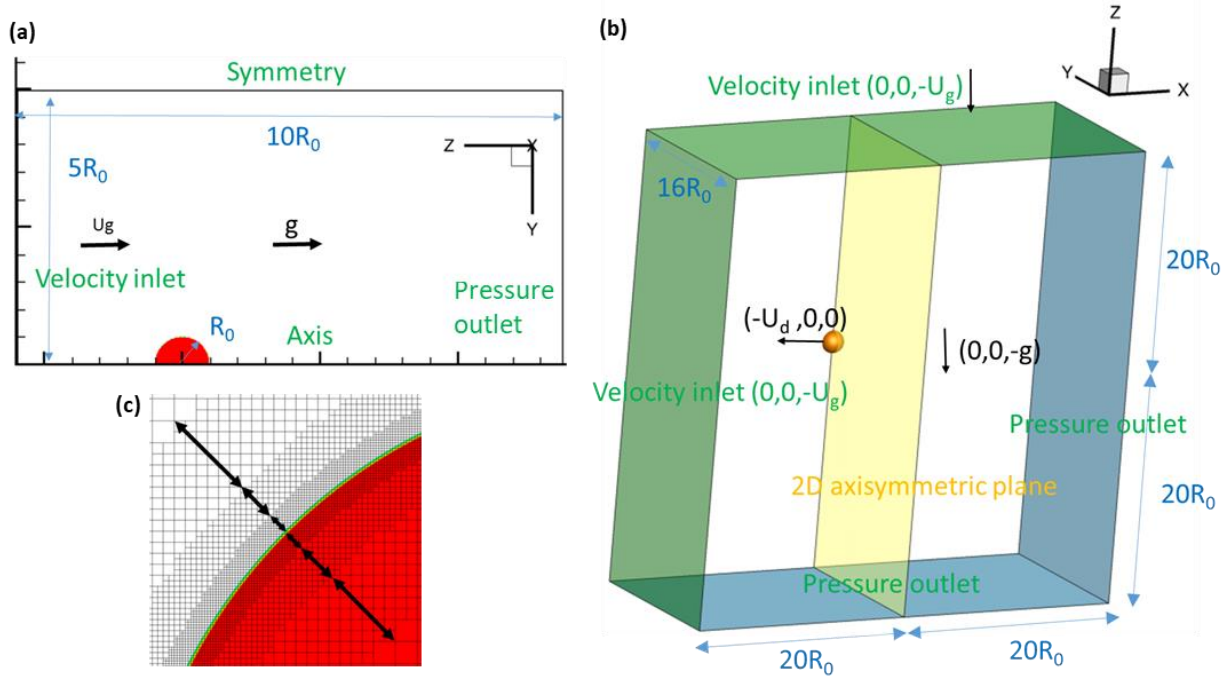


Figure 2. Computational domain of a) 2D axisymmetric and b) 3D simulations. c) Levels of local refinement around the liquid-gas interface.

The representative engine conditions for light Diesel and HFO fuelled engines are listed in Table 1 in which the effect of cylinder pressure and temperature is reflected in the gas properties; the data of Table 1 are used to draw the engine conditions in Figure 1. For the light Diesel fuelled engines the droplet diameters and velocities are based on the publication of [21], while the liquid properties are calculated from [40] for $T_L=323\text{K}$. For the HFO fuelled engines the droplet velocities are also based on [21], while liquid properties were taken from [41] for $T_L=353\text{K}$. In both engine types the operating We numbers range from $O(1)$ up to $O(1000)$, whereas the Oh numbers are significantly greater in HFO fuelled engines owed to the high viscosity of heavy fuel oil.

Table 1: Representative conditions for light Diesel and HFO fuelled compression ignition engines based on [21, 40, 41].

| | T_L [K] | ρ_l [kg/m ³] | μ_l [kg/(s·m)] | ρ_g [kg/m ³] | μ_g [kg/(s·m)] | σ [N/m] | U_g [m/s] | D_0 [μm] |
|--------------|-----------|-------------------------------|--------------------|-------------------------------|-------------------------|----------------|-------------|-------------------------|
| Light Diesel | 323 | 816 | 0.0021 | 15-40 | $3.7-4.6 \cdot 10^{-5}$ | 0.027 | 10-100 | 10-100 |
| HFO | 353 | 954 | 0.0537 | 13-30 | $3.7-4.6 \cdot 10^{-5}$ | 0.026 | 10-100 | 50-125 |

The conditions of the simulated cases are presented in Table 2. The fuel properties considered are based on published experimental data [4, 41], while the ambient gas properties range from atmospheric ($P=1\text{bar}$ and $T=298\text{K}$) up to those encountered in Diesel engines (i.e. $P=30\text{-}100\text{bar}$ and $T_g=780\text{-}1100\text{K}$). Cases 1-4 for Diesel droplets are used for model validation (they do not represent engine conditions) and the numerical results are compared against the experimental data of Arcoumanis et al. [3], Liu and Reitz [4] and Lee and Reitz [5]. The examined We numbers in these cases range from 14 up to 264, covering a wide range of breakup regimes, while the density ratio changes from 695 ($P=1\text{bar}$) down to 79 ($P=9.2\text{bar}$). The Oh number in cases 1-4 is lower than 0.04 so its effect on the phenomenon is considered to be insignificant [1]. Cases 5-18 correspond to the parametric studies of this work for the case of Diesel and HFO droplets; all cases with HFO correspond to engine conditions except for cases 14 and 15. The examined We numbers range from 14 up to 254, the Oh numbers from 0.011 to 1.525 and the density ratio from 30 to 816. All cases are simulated in a 2D axisymmetric domain with the exception of case 2, which is also simulated in a 3D computational domain. The Reynolds number in the simulations ranges from 422 to 5761 which is less than the critical Reynolds number ($Re_{crit}=2*10^5$) for the transition to turbulent flow in flow around solid spheres [42]. Moreover, the simulation can be regarded as DNS (Direct Numerical Simulation), since the cell size at the interface region is up to 4 times smaller than the Kolmogorov length scale ($\sim(\nu^3/U_g^3*D_0)^{1/4}$), while the timestep is up to 20 times smaller than the corresponding turbulence timescale ($\sim(\nu*D_0/U_g^3)^{1/2}$). This consideration is common in previous numerical studies on droplet breakup with high Reynolds numbers [22, 24, 43, 44].

Table 2: Operating conditions for the examined cases.

| Case | Fuel | D_0 [μm] | P [bar] | We | Re | Oh | ϵ | Predicted Breakup regime | Examined parameter | Relevant experiment |
|------|--------|-------------------------|-----------|------|------|-------|------------|--------------------------|--------------------|---------------------|
| 1 | Diesel | 2400 | 1 | 14 | 1540 | 0.011 | 695 | Bag | } We at low Oh | [3] |
| 2 | Diesel | 198 | 1 | 54 | 864 | 0.038 | 695 | Multi-bag | | [4] |
| 3 | Diesel | 198 | 1 | 254 | 1867 | 0.038 | 695 | Sheet-thinning | | [4] |
| 4 | Diesel | 184 | 9.2 | 264 | 5761 | 0.039 | 79 | Sheet-thinning | } Low ϵ | [5] |

| | | | | | | | | | | | |
|----|--------|------|-----|-----|------|-------|-----|----------------|---|--------------------------------------|---|
| 5 | Diesel | 2324 | 30 | 14 | 2362 | 0.011 | 72 | Bag | } | <i>Oh</i> at <i>We</i> =14 | - |
| 6 | HFO | 125 | 30 | 14 | 667 | 0.965 | 72 | Deformation | | | - |
| 7 | HFO | 50 | 30 | 14 | 422 | 1.525 | 72 | Deformation | | | - |
| 8 | Diesel | 195 | 30 | 54 | 1343 | 0.038 | 72 | Sheet-thinning | } | <i>Oh</i> at <i>We</i> =54 | - |
| 9 | HFO | 125 | 30 | 54 | 1310 | 0.965 | 72 | Deformation | | | - |
| 10 | HFO | 50 | 30 | 54 | 828 | 1.525 | 72 | Deformation | } | <i>Oh</i> at <i>We</i> =254 | - |
| 11 | Diesel | 195 | 30 | 254 | 2912 | 0.038 | 72 | Sheet-thinning | | | - |
| 12 | HFO | 125 | 30 | 254 | 2841 | 0.965 | 72 | Sheet-thinning | | | - |
| 13 | HFO | 50 | 30 | 254 | 1797 | 1.525 | 72 | Sheet-thinning | } | High ϵ at <i>We</i> =54 | - |
| 14 | HFO | 125 | 1 | 54 | 769 | 0.965 | 816 | Bag | | | - |
| 15 | HFO | 50 | 1 | 54 | 486 | 1.525 | 816 | Bag | } | Low ϵ at <i>Oh</i> =0.96 | - |
| 16 | HFO | 125 | 100 | 14 | 830 | 0.965 | 30 | Deformation | | | - |
| 17 | HFO | 125 | 100 | 54 | 1630 | 0.965 | 30 | Deformation | | | - |
| 18 | HFO | 125 | 100 | 254 | 3536 | 0.965 | 30 | Sheet-thinning | | | - |

3 Results and discussion

3.1 Model validation (Diesel droplets)

3.1.1 Bag breakup regime (*We*=14)

The results from the simulation of case 1 are compared against the experimental data from the publication of Arcoumanis et al. [3]. Figure 3 illustrates the temporal evolution of droplet shape (using the VOF iso-value of 0.5) and the predicted deformation in the two axes. The droplet deforms into an oblate shape up to the time of approximately $1.4t_{sh}$, as it grows in the streamwise direction and thins in the cross-stream one. Then, the bag starts to form up to $t=1.75t_{sh}$, while throughout this period the deformation increases in both directions. Eventually the bag breaks into small fragments at $t=1.85t_{sh}$. The evolution of droplet shape and the droplet deformation are correctly predicted by the model up to the time of breakup initiation. The main difference between the simulation and the experiment lies on the prediction of the breakup initiation time, which is equal to $1.85t_{sh}$ in the simulation compared to $2.93t_{sh}$ in the experiment. Nonetheless, the predicted breakup time of $1.85t_{sh}$ is located within the proposed boundaries given by Pilch and Erdman [45] and Dai and Faeth [46] (see Figure 12 later in this section).

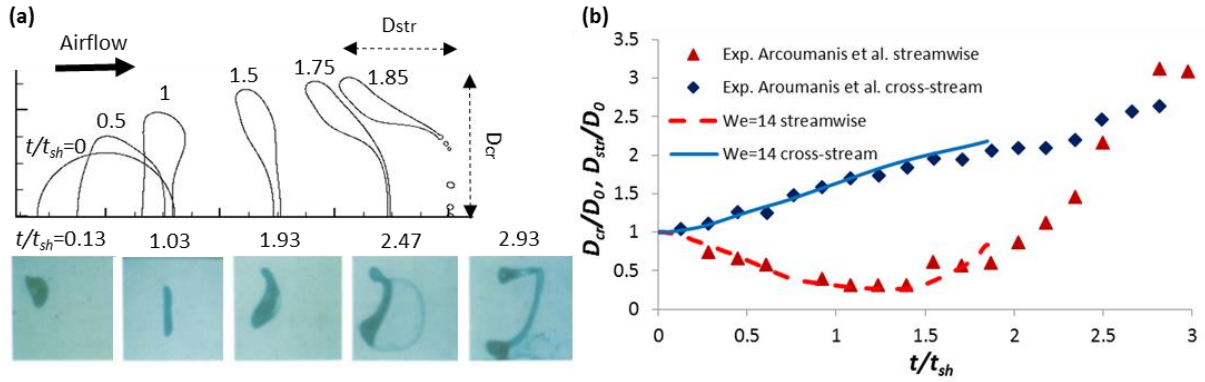


Figure 3. Temporal evolution of a) droplet shape and b) deformation for the simulation of case 1 ($We=14$) and the experiment of Arcoumanis et al. [3].

3.1.2 Multimode breakup regime ($We=54$)

The droplet shapes for case 2 with the intermediate We number of 54 are presented in Figure 4. This includes the predicted droplet shapes for (a) the 2D axisymmetric, (b) the 3D simulations (X-Z plane), as well as the corresponding experimental photos of Liu and Reitz [4] in (c). Up to the time of $1.4t_{sh}$ the droplet deforms into an oblate shape similar to case 1 (bag breakup), followed by the growth of a toroidal bag at the periphery of the drop rather than at the centre as in case 1 ($We=14$). This breakup mode pertains to the multi-bag (multimode) breakup regime instead of the bag reported in the experiment, as shown in Figure 4c: the drop takes an oblate shape (droplet no. 3 in image i), followed by the formation of the bag (droplet no. 4 in image i) and the subsequent breakup into small fragments (droplet no.4 in image ii). Nevertheless, the predicted multimode breakup is in accordance with the breakup regions in the $Oh-We$ map of Hsiang and Faeth [12] (Figure 1) for the examined We and Oh numbers. In order to further investigate if this discrepancy is ought to 3D phenomena and also to assess the effect of cross-stream droplet motion, corresponding 3D simulations have been conducted and presented in Figure 4b. The 3D simulations reveal a quite similar behaviour with the 2D ones, apart from a predicted slightly later breakup initiation time ($1.8t_{sh}$ compared to $1.65t_{sh}$ in the 2D simulation) and a slight tilting of the droplet. The latter is ought to the declination of the relative drop-gas velocity from the vertical direction (Figure 4b) and it is not affecting the general model performance. A more

representative view of the 3D simulation is presented in Figure 5 showing the formation of two bags instead of the torus predicted by the 2D simulations.

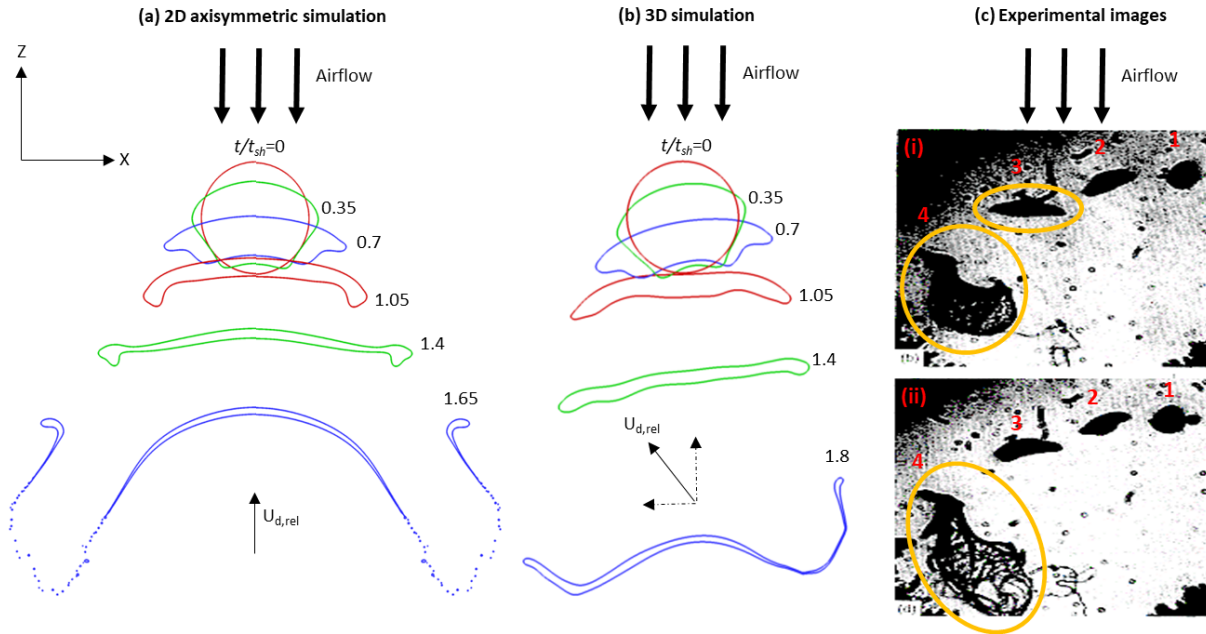


Figure 4. Temporal evolution of droplet shape for a) the 2D axisymmetric simulation of case 2 ($We=54$), b) the 3D simulation of case 2, and c) the experiment of Liu and Reitz [4].

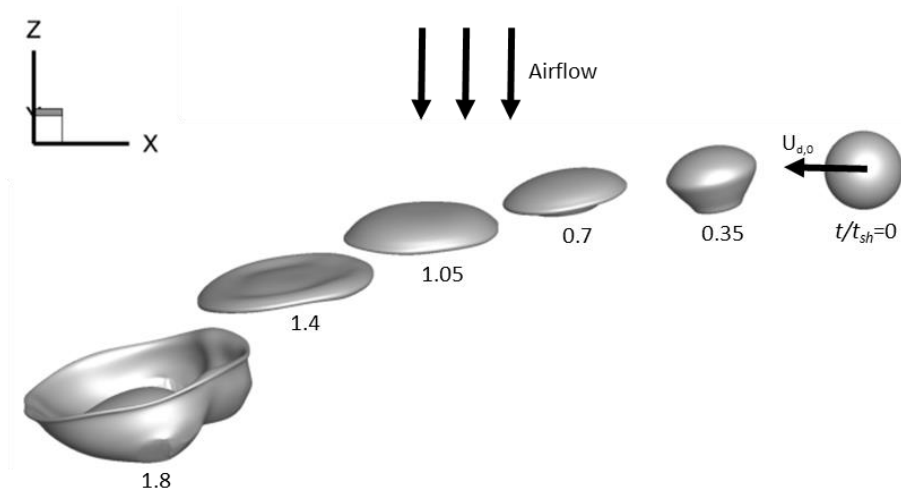


Figure 5. Temporal evolution of droplet shape from the 3D simulation of case 2 ($We=54$).

Regarding the quantitative comparison between the simulation of case 2 and the experiment of Liu and Reitz [4] the graph of the deformation as function of the distance travelled along the cross-stream

direction is given in Figure 6. The deformation increases gradually with the distance travelled, as depicted both in the simulations and the experiment.

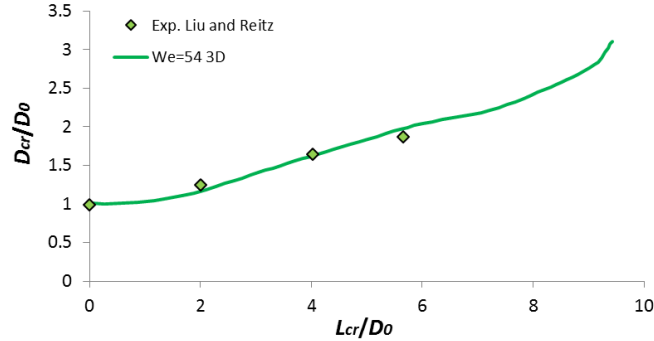


Figure 6. Droplet deformation for the simulation of case 2 ($We=54$) and the experiment of Liu and Reitz [4] as function of the distance travelled in the cross-stream direction.

For the examined conditions of case 2 ($Re=864$), vortex shedding behind the droplet should normally be present; for spherical droplets this is observed for Re numbers in the range 400 up to $3.5 \cdot 10^5$ [42]. The frequency f of the vortex detachment is generally expressed through the Strouhal number ($St = fD_0/U_{rel,0}$) which is equal to 0.2 for solid spheres [42] and 0.13 for solid disks [47] based on the Re number of the simulation. This phenomenon can be captured only in the 3D simulations and this is evident from the streamlines of the relative velocity field in Figure 7, where alternating vortices detach from the droplet surface in the symmetry plane (X-Z). According to Sakamoto and Haniu [48] the vortices in solid spheres with $Re > 480$ are detached periodically from a point at the wake of the droplet that rotates around an axis through the centre of the sphere. Achenbach [49] states that there are four detachment points at the wake of the drop in a helical formation and defines the vortex shedding period as the time between two consecutive detachments. Due to the adoption of the symmetry boundary condition, asymmetrically forming vortices cannot be captured with the current setup. Nevertheless, an indication of the vortex shedding period can be estimated to be equal to the half time between the separation of two consecutive vortices in the X-Z plane (at $t=0.7t_{sh}$ and $t=1.1t_{sh}$). This period results in a Strouhal number equal to 0.19, which is a value slightly less than the value of solid

spheres. It should be noted that although the symmetry boundary condition is not suitable for predicting the 3D gas flow structure its effect on the liquid phase deformation is minimal.

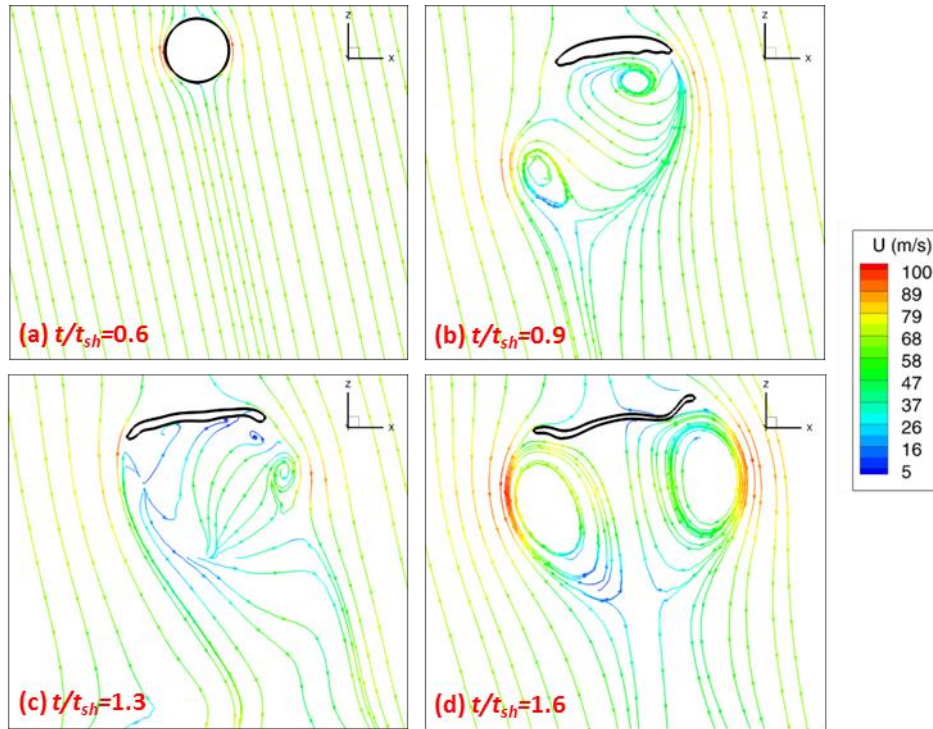


Figure 7. Vortex shedding in the 3D simulation of case 2 at various time instances (streamlines coloured with velocity magnitude).

3.1.3 Sheet-thinning breakup regime ($We=254$ and 264)

Turning now to the cases subjected to sheet-thinning breakup mode, the temporal evolution of droplet shape for cases 3 and 4, as well as the corresponding experimental photographs of Liu and Reitz [4] and Lee and Reitz [5] are illustrated in Figure 8. These cases have similar We numbers (254 compared to 264), but different density ratios (695 compared to 79). The sheet-thinning breakup modes predicted for the two cases are in agreement with the corresponding experimental data. The drop initially deforms into a disk-like shape (this is a common feature for all breakup modes), followed by the formation of a thin liquid sheet at the periphery of the drop. This liquid sheet forms ligaments which are eventually detached from the droplet during the breakup process, as observed in both the

numerical predictions as well as the experimental images (droplet no. 3). The breakup time is lower in the case with $\varepsilon=79$ compared to the one with $\varepsilon=695$, equal to $0.8t_{sh}$ against $0.95t_{sh}$ respectively.

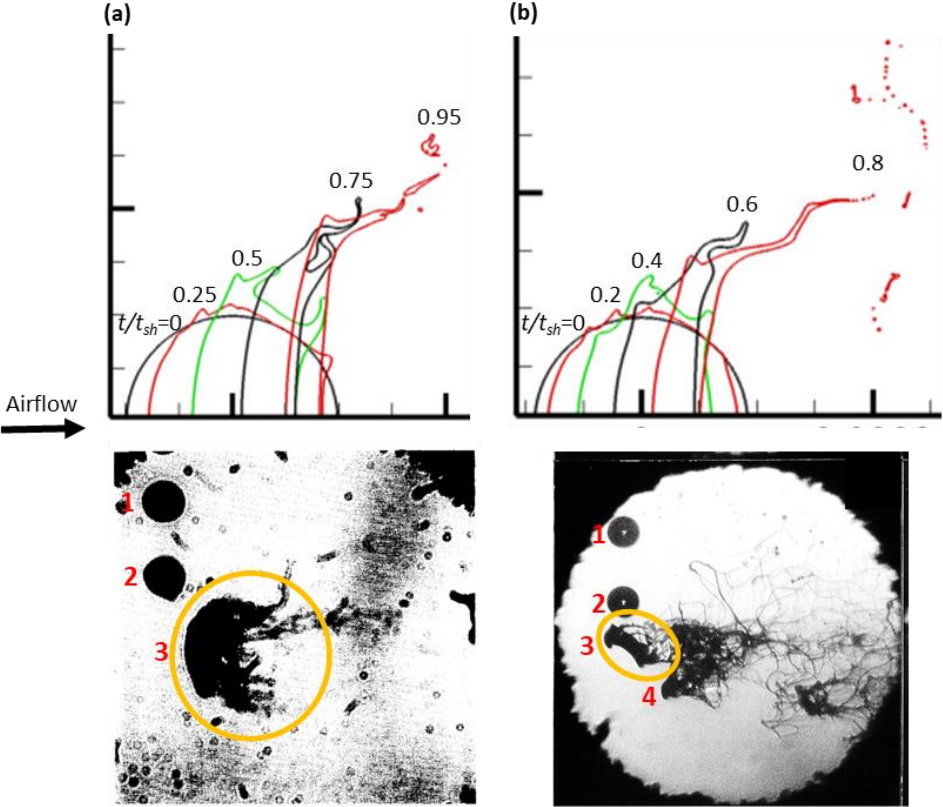


Figure 8. Temporal evolution of droplet shape for a) case 3 ($We=254$, $\varepsilon=695$) and the experiment of Liu and Reitz [4] and b) case 4 ($We=264$, $\varepsilon=79$) and the experiment of Lee and Reitz [5].

The cross-stream deformation as function of the distance travelled in the cross-stream direction for case 3 ($We=254$) and the corresponding experimental data of Liu and Reitz [4] are shown in Figure 9. It is observed that the deformation increases with the distance similar to case 2, while there is also a very good agreement between the simulation and the experiment.

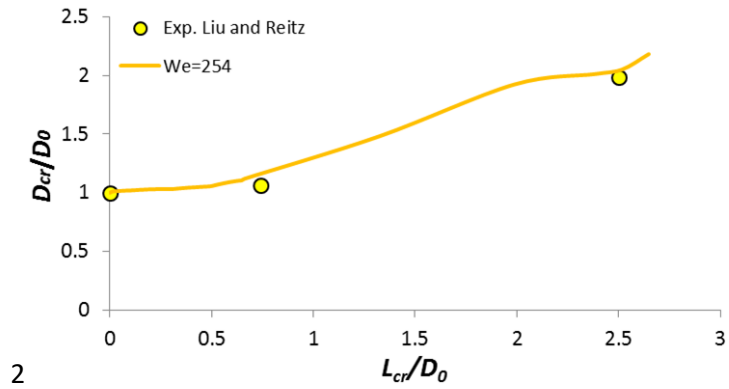


Figure 9. Droplet deformation for the simulation of case 3 ($We=254$) and the experiment of Liu and Reitz [4] as function of the distance travelled in the cross-stream direction.

3.1.4 Overall assessment of the effect of We number

In this section, the overall effect of the We number for all the four validation cases is addressed. Starting with the temporal evolution of the cross-stream droplet deformation this is presented in Figure 10. It is observed that the rate of deformation increases with the We number in agreement with the experiment of [7] and the numerical studies of [18] and [20].

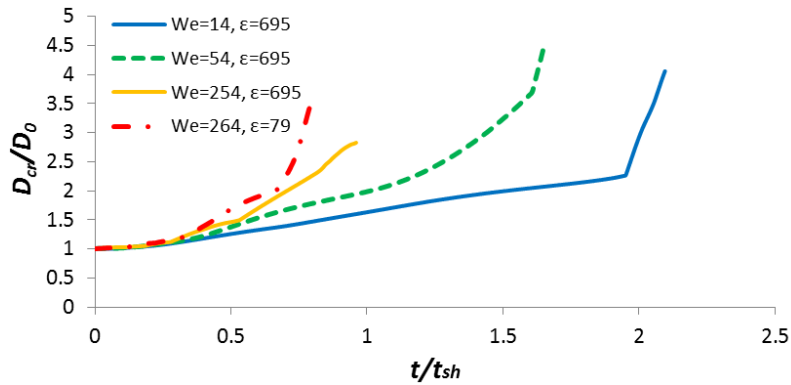


Figure 10. Temporal variation of the cross-stream deformation for all validation cases.

The next parameter that is investigated is the non-dimensional droplet velocity $U_d/(U_{g,0}-U_d)$ which is presented in Figure 11 along with the experimental results of Dai and Faeth [46] ($We=15-150$ and $\epsilon=680-850$). As seen, the dimensionless character of droplet velocity is confirmed for all cases examined. Only the case with $\epsilon=79$ shows a small deviation from the experimental data probably due

to the small density ratio compared to the large density ratios examined in the experiments; the Re numbers between those cases, differ also a lot.

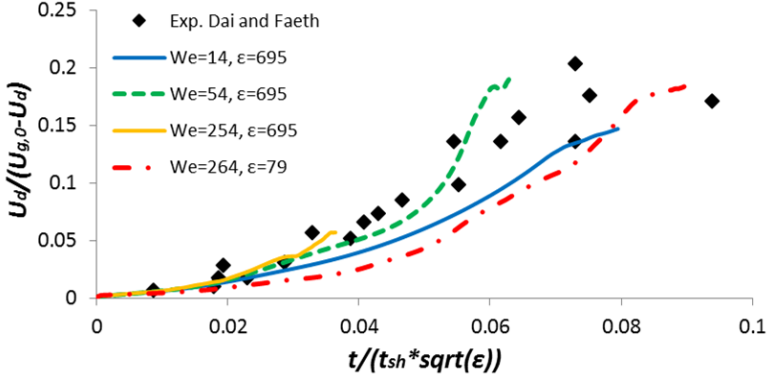


Figure 11. Non-dimensional droplet velocity as function of modified time for all validation cases and the experiment of Dai and Faeth [46].

Regarding the non-dimensional breakup initiation time, this is presented in Figure 12 as a function of the We number along with the correlations suggested by Pilch and Erdman [45] and Dai and Faeth [46]. The breakup initiation time decreases with increasing We number and the predicted breakup times are located within the proposed experimental boundaries; the low We number cases (bag and multi-bag) seem to be closer to the correlation of Dai and Faeth [46], whereas the high We number cases (sheet-thinning) are closer to the correlation of Pilch and Erdman [45].

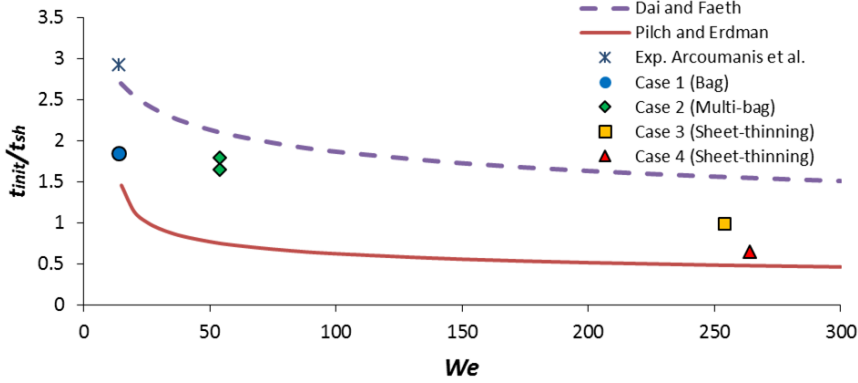


Figure 12. Predicted breakup initiation time as function of We number for validation cases along with the experimental correlations of Pilch and Erdman [45] and Dai and Faeth [46].

3.2 Parametric study (HFO and Diesel droplets)

Following model validation against experimental data for Diesel fuel, the numerical model is utilized to investigate the aerodynamic breakup of HFO ($Oh=0.96$ and 1.53) and Diesel droplets ($Oh < 0.04$) for density ratios representative of Diesel engines ($\varepsilon=30$ and 72), as well as at atmospheric conditions ($\varepsilon=816$). In the following sections, initially the temporal evolution of droplet shape for various combinations of We , Oh and ε numbers is presented followed by details about the droplet deformation, drag coefficient and breakup initiation time. The main distinction between Diesel and HFO, in terms of properties, can be relected to the range of Oh numbers characterizing their deformation. For that reason, the following subsections refer to the effect of Oh on them.

3.2.1 Effect of Oh and ε numbers on the breakup mode

Starting with a low density ratio of 72 , the effect of increasing Oh number on the droplet deformation is highlighted for three We numbers (14 , 54 and 254). The temporal evolution of droplet shape for these conditions is presented in Figure 13. For We numbers of 14 (cases 5-7) and 54 (cases 8-10) the increase of Oh number from less than 0.04 to 0.96 and further to 1.53 leads to the change of the bag breakup mode for low Oh to a non-breakup oscillatory deformation for higher Oh numbers. For We number of 14 , this transition is in accordance with the boundaries proposed by Hsiang and Faeth [12] (Figure 1a), while for $We=54$ a bag breakup mode should have been predicted instead of the deformation. Nevertheless, the boundaries between the different breakup modes in Figure 1a have been developed for high density ratios (>580), while in the current simulations the density ratio is equal to 72 . Such differences are further discussed in the next paragraph where the effect of density ratio on the breakup mode is investigated. Turning now to the examination of cases with We number equal to 254 (cases 11-13), it is observed in Figure 13 that the increase of Oh number does not affect the breakup mode, which remains sheet-thinning for all the examined Oh numbers, in agreement with Hsiang and Faeth [12]. The temporal evolution of droplet shape for the Oh number of 1.53 shows that

before the onset of breakup a portion of the liquid mass is concentrated at the centre of the droplet similar to the bag-stamen breakup mode [17], probably due to the high viscosity of HFO.

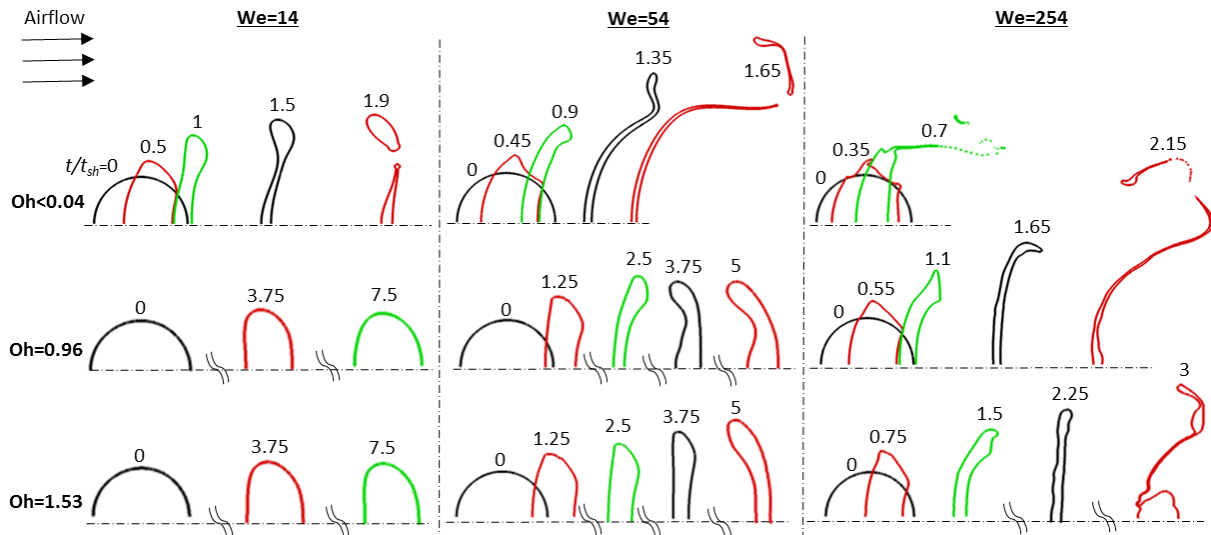


Figure 13. Temporal evolution of droplet shape for three We numbers and three Oh numbers ($\epsilon=72$).

For the We number of 54 the breakup of HFO droplets is further investigated under atmospheric conditions (cases 14 and 15 with $\epsilon=816$) in order to examine the effect of density ratio on the breakup mode. In Figure 14 the temporal evolution of droplet shape is presented for $Oh=0.96$ and two density ratios of 72 (case 9) and 816 (case 14). It is observed that the single change in density ratio from 72 to 816 resulted in the change of the breakup mode from deformation to multi-bag. This is in accordance with the findings of Aalburg [19], who stated that the critical We number increases with decreasing density ratio. Although Aalburg [19] found that the change of the critical We number is significant when the density ratio is below 32, the examined cases are very close to the boundaries of the breakup regime and this can affect the breakup mode.

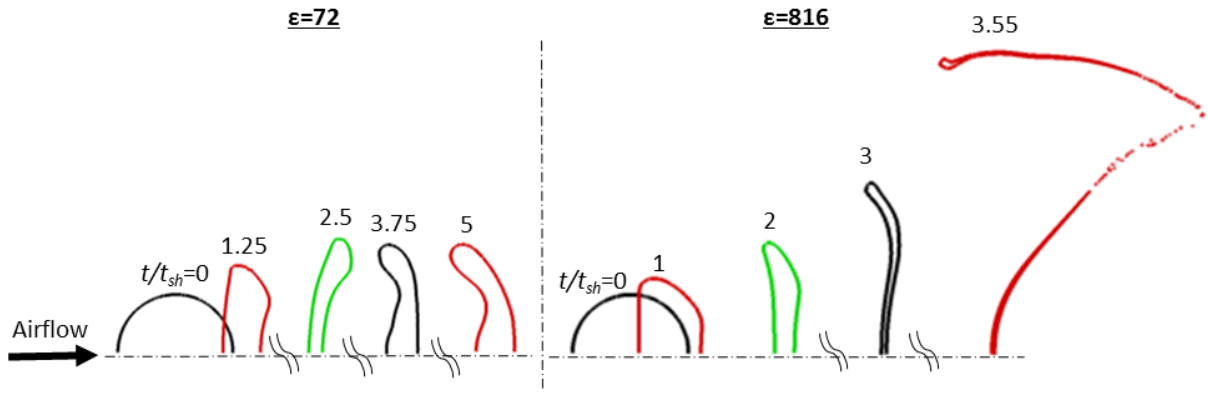


Figure 14. Temporal evolution of droplet shape for $We=54$, $Oh=0.96$ and two density ratios (cases 9 and 14).

3.2.2 Effect of Oh number on droplet deformation, liquid surface area and drag coefficient

Turning now to the quantitative effect of Oh number on the breakup process, its effect on the parameters of droplet deformation, drag coefficient and liquid surface area is investigated, the latter of which is a quantity that plays an important role in combustion systems and it is difficult to be measured experimentally. Figure 15 presents the temporal evolution of the droplet deformation for three Oh numbers (0.038, 0.96 and 1.53) and two $We-\epsilon$ combinations, i.e (a) 54-694 (cases 2, 14 and 15) and (b) 254-72 (cases 11-13). The streamwise (D_{str}) and cross-stream (D_{cr}) deformations follow the same trend as in previous cases, i.e. the streamwise deformation initially decreases due to drop flattening, followed by an increase owed to the formation of the bag or sheet, while the cross-stream one increases during the whole duration of the process. The increase of Oh number results in a lower deformation rate, in accordance with the experiments of [9] and the numerical studies of [18], [20], [21] and [23].

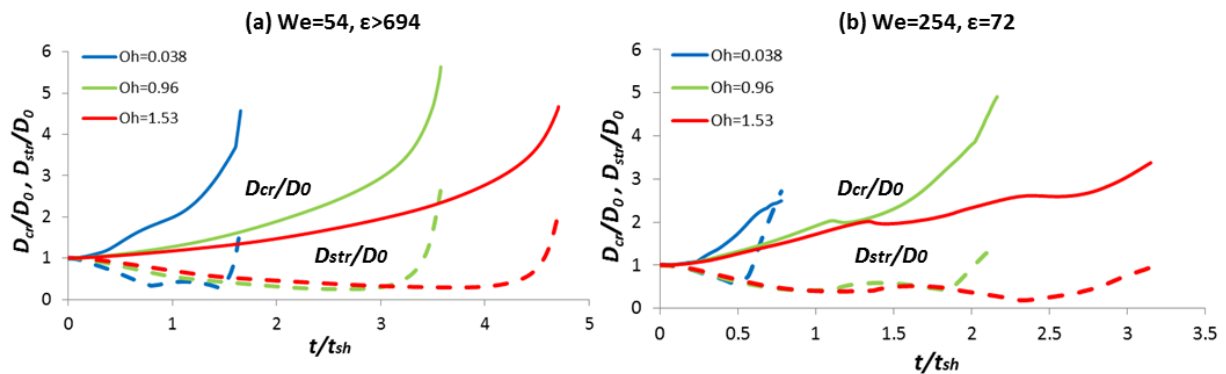


Figure 15. Temporal evolution of both main axis deformation (D_{cr} , D_{str}) for three Oh numbers and a) $We=54$ and $\epsilon>694$ (cases 2, 14 and 15), and b) $We=254$ and $\epsilon=72$ (cases 11-13). The solid lines correspond to the cross-stream deformation and the dashed ones to the stream-wise one.

The temporal evolution of the liquid surface area for the same conditions is presented in Figure 16. Initially an almost linear increase of the dimensionless liquid surface area is predicted during the drop flattening, followed by a steep increase owed to the formation of the bag. For the higher We number cases as depicted in Figure 16b a smoother increase rate is observed, as a liquid sheet is formed instead of a bag. Generally, the liquid surface area increases several times by the onset of breakup. Similar to the rate of drop deformation, the increase rate of liquid surface area also decreases with increasing Oh number.

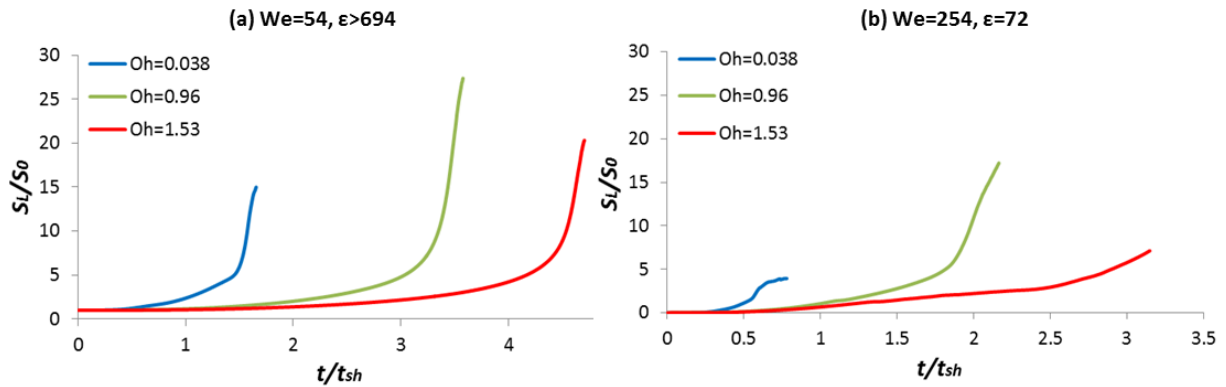


Figure 16. Temporal evolution of liquid surface area for three Oh numbers and a) $We=54$ and $\epsilon>694$ (cases 2, 14 and 15), and b) $We=254$ and $\epsilon=72$ (cases 11-13).

Another parameter that can be useful in spray codes following Lagrangian approaches to simulate the spray evolution, is the droplet's drag coefficient (C_d); this can be calculated with the aid of the droplet momentum equation:

$$m \frac{d}{dt} (U_d(t)) = \frac{1}{2} C_d(t) \rho_g U_{rel}^2(t) A_f(t) \quad (3)$$

The left hand side of eq.(3) is the rate of droplet momentum change and the right hand side is the drag force exerted on it; the effect of all other forces that act on the droplet (virtual mass, Basset and other forces) have been incorporated in the drag coefficient, similar to previous numerical studies [20, 24, 26, 44]. By rearranging equation (3) and using the expressions for droplet mass m and relative velocity U_{rel} , as well as the definition of density ratio (eq. (1)), we get the final expression for C_d in eq.(4):

$$C_d(t) = \frac{\frac{4}{3} D_0 \varepsilon \frac{dU_d(t)}{dt} \frac{A_f(0)}{A_f(t)}}{(U_g - U_d(t))^2} \quad (4)$$

The drag coefficient changes in time as the droplet-gas relative velocity decreases and the droplet shape changes from spherical to a disk-like. The temporal variation of the drag coefficient is presented in Figure 17 for three cases (2, 14 and 15) with $We=54$, $\varepsilon>694$ and Oh numbers 0.038, 0.96 and 1.53. In all cases the C_d at the beginning of the simulation reaches very high values, owed to the highly unstable flow field during this period, followed by a steep decrease similar to the findings of [21, 23]. During the rest of the process the drag coefficient increases steadily due to droplet acceleration up to the point of breakup initiation, where it decreases abruptly as also found in [23]. Moreover, from the same figure it is observed that as the Oh number is increased the drag coefficient decreases, in agreement with the findings of [20, 21]. Given that the breakup mode is the same for all cases (bag breakup) and that the rate of deformation is higher for lower Oh numbers, the cases with smaller Oh numbers deform faster into oblate shapes (disk-like); these shapes result in higher accelerations and drag coefficients.

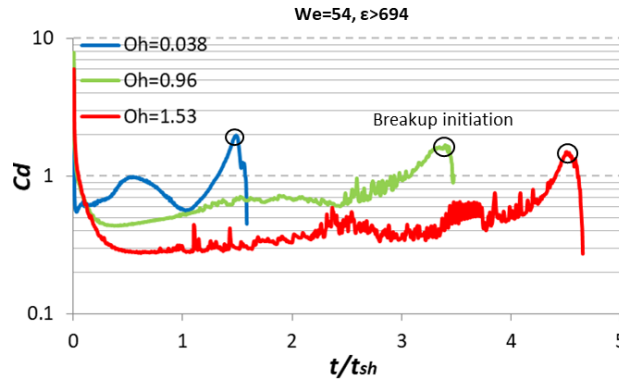


Figure 17. Temporal evolution of drag coefficient for cases 2, 14 and 15 (various Oh numbers).

The parametric study of Oh number reveals that the less viscous fuels (e.g. Diesel over HFO in this study) promote the breakup process as the rate of deformation, liquid surface area and drag coefficient are larger than those of the viscous fuels (e.g. HFO).

3.2.3 Effect of Oh number on the breakup initiation time

This section investigates the effect of Oh number on the time required for the initiation of breakup. In all examined cases the increase of Oh number resulted in an increase of the breakup initiation time (or even ceased breakup) in agreement with the experimental study of Hirahara and Kawahashi [50]. In Strotos et al. [37] the breakup initiation time was correlated as a function of We and Re numbers (valid for low Oh and high ϵ numbers), while later Stefanitsis et al. [29] proposed a correction factor to account also for changes in the density ratio ϵ . Based on the results of the present parametric study, an additional correction factor is proposed which accounts also for the effect of Oh number, apart from those of We , Re and ϵ ; the resulting equation is eq.(5). This term was inspired by the correlations of Gel'fand et al. [11] and Pilch and Erdman [45] and is extracted following a best-fitting procedure for the conditions of cases presented in Table 2 and two additional cases (with $Oh=0.2$ and $Oh=3$ which are not presented in the current work). The predicted term has the same general form as in Gel'fand et al. [11] i.e. $(1+A \cdot Oh^B)$, with A and B constants.

$$\frac{t_{init}}{t_{sh}} = 8.95 \cdot (We^{-0.352} Re^{-0.086}) \cdot \left(\frac{1}{1 + \varepsilon^{-0.5}} \right) \cdot (1 + 2.36 Oh^{0.93}) \quad (5)$$

The predicted breakup initiation times from equation (5) are shown in Figure 18 along with the actual times calculated from the simulations, for the whole range of examined conditions in this paper and the publications of [29] (Diesel), [38] (n-heptane) and [37] (n-decane). In addition, the lines for $\pm 20\%$ deviation are also presented. In almost all cases the predicted breakup initiation times from equation (5) lie within a maximum deviation of 20% from the corresponding ones of the simulations.

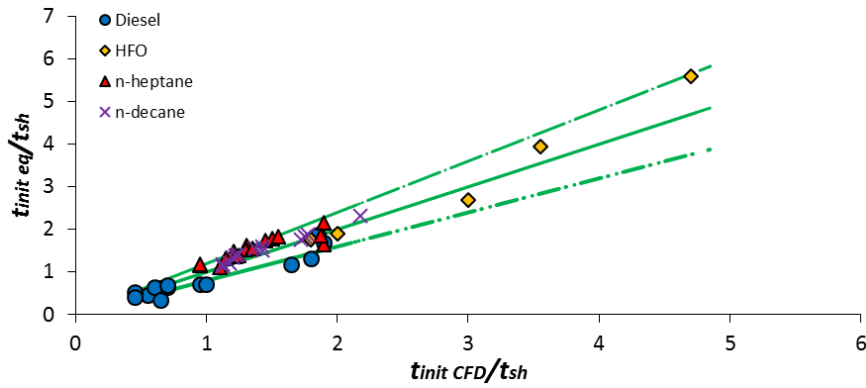


Figure 18. Breakup initiation time as predicted by eq. (5) (data points) and the simulations (straight lines).

4 Conclusions

The present study investigates numerically the aerodynamic breakup of Diesel and heavy fuel oil droplets under liquid to air density ratios ranging from 30 up to 816. The results of the numerical model are compared against published experimental data for Diesel fuel in conditions corresponding to We numbers from 14 up to 264, two density ratios (79 and 695) and low Oh numbers (<0.04). It is proved that the model is capable of predicting with satisfactory accuracy the breakup modes in three breakup regimes, i.e. a) bag, b) multimode and c) sheet-thinning. In addition, the temporal evolution of droplet deformation and non-dimensional velocity are in agreement with the experimental data. The increase of We number resulted in an increase also in the rate of deformation of the droplets. The predicted breakup initiation times lie within the limits proposed by Pilch and Erdman [45] and Dai and Faeth [46],

with the lower We numbers (bag and multi-bag regimes) being closer to the correlation of Dai and Faeth [46], whereas for the higher We numbers (sheet-thinning) the correlation of Pilch and Erdman [45] is more accurate. Furthermore, the 3D simulations of droplet breakup indicate the appearance of vortex shedding simultaneously with the breakup process with a roughly estimated frequency slightly less than the one for a flow around solid spheres.

A parametric study with Diesel and HFO droplets investigating the effect of Oh number and density ratio on the breakup process has been also performed. The change of operating fuel from Diesel to HFO resulted in much higher Oh numbers (along with the change in diameter the Oh increased from 0.04 to 0.96 and 1.53), while the We numbers were kept constant (14, 54 and 254). Two out of the three breakup modes were altered into oscillatory deformation without breakup, while the sheet-thinning regime remain unchanged. Furthermore, it was observed that changing the density ratio from 72 to 816 resulted in the alternation of the breakup mode from deformation to bag breakup. In addition, the increase of Oh number resulted in a decrease in the rate of deformation, liquid surface area and drag coefficient meaning that the breakup process is hindered when using high viscous fuels such as HFO. On the other hand, the breakup initiation time increased with the increase of Oh number and a correction in the equation for the prediction of breakup initiation time is proposed to account for this effect.

Acknowledgements

Financial support from the MSCA-ITN-ETN of the European Union's H2020 programme, under REA grant agreement n. 675676 is acknowledged.

Appendix A. Indication of the effect of heating and evaporation on the breakup of HFO droplets

In the conditions of cases 6-18 a gas temperature in the range of 780-1100K is assumed in order to resemble the conditions exhibited in Diesel engines. In these high temperatures evaporation and heating of the droplet takes place, which is not accounted for in the current model and will be

implemented in future works. Nevertheless, an indication about the effect of heating and evaporation processes on the breakup can be assessed utilizing the OD model for the heating and evaporation of droplets undergoing breakup as proposed in Strotos et al [37]. It should be noted that this model was originally developed for the evaporation of volatile low viscosity fuels at atmospheric pressure. Its use in the current work, without any modification, for high pressure conditions and low volatility fuel (HFO) acts as an indication for the effect of heating and evaporation. The properties of HFO have been taken in their majority from [41], while for the thermal conductivity and the heat capacity the properties of n-hexadecane were used [51, 52] since they resemble those of HFO. The temporal evolution of droplet surface is calculated based on the data from the current simulations and not the proposed correlations of [37].

The OD evaporation model is utilized to predict the evaporated mass and the droplet temperature at the time equal to t_{sh} ; the actual time of breakup cannot be used instead, as most examined cases experience only deformation and not breakup. For all cases the evaporated mass up to $t = t_{sh}$ is less than $10^{-4}\%$ of the initial droplet mass and therefore it can be considered negligible; this is attributed to the very low vapour pressure of HFO (in the order of a few Pa in the initial fuel temperature of 353K). The increment of droplet temperature (ΔT_m) at $t = t_{sh}$ is presented for all cases with HFO as function of the We number in Figure A1. It is seen that the temperature rise increases with the gas temperature and decreases with the We number and the droplet diameter. This temperature increase affects the properties of the fuel and is important especially for the viscosity and surface tension, which alter the We and Oh numbers. The percentage differences from their initial values at $t = t_{sh}$ are estimated for these parameters: for the surface tension they are found less than 1% for all cases with HFO, while for the viscosity they reach values as high as 17%.

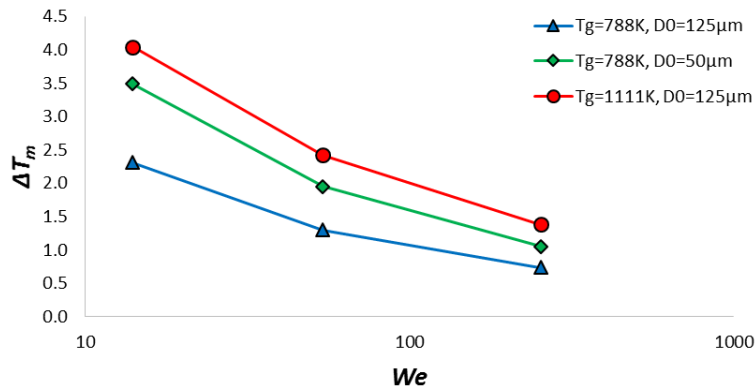


Figure A1. Droplet mean temperature increase at $t = t_{sh}$ as function of the We number due to the effect of heating (HFO).

References

- [1] Guildenbecher, D. R., López-Rivera, C., and Sojka, P. E., 2009, "Secondary atomization," *Experiments in Fluids*, 46(3), pp. 371-402.
- [2] Nicholls, J. A., and Ranger, A. A., 1969, "Aerodynamic shattering of liquid drops," *AIAA Journal*, 7(2), pp. 285-290.
- [3] Arcoumanis, C., Khezzar, L., Whitelaw, D. S., and Warren, B. C. H., 1994, "Breakup of Newtonian and non-Newtonian fluids in air jets," *Experiments in Fluids*, 17(6), pp. 405-414.
- [4] Liu, Z., and Reitz, R. D., 1997, "An analysis of the distortion and breakup mechanisms of high speed liquid drops," *International Journal of Multiphase Flow*, 23(4), pp. 631-650.
- [5] Lee, C. H., and Reitz, R. D., 2000, "An experimental study of the effect of gas density on the distortion and breakup mechanism of drops in high speed gas stream," *International Journal of Multiphase Flow*, 26(2), pp. 229-244.
- [6] Lee, C. S., and Reitz, R. D., 2001, "EFFECT OF LIQUID PROPERTIES ON THE BREAKUP MECHANISM OF HIGH-SPEED LIQUID DROPS," 11(1), pp. 1-19.
- [7] Park, S. W., Kim, S., and Lee, C. S., 2006, "Breakup and atomization characteristics of mono-dispersed diesel droplets in a cross-flow air stream," *International Journal of Multiphase Flow*, 32(7), pp. 807-822.
- [8] Kim, S., Hwang, J. W., and Lee, C. S., 2010, "Experiments and modeling on droplet motion and atomization of diesel and bio-diesel fuels in a cross-flowed air stream," *International Journal of Heat and Fluid Flow*, 31(4), pp. 667-679.
- [9] Hinze, J. O., 1955, "Fundamentals of the hydrodynamic mechanism of splitting in dispersion processes," *AIChE Journal*, 1(3), pp. 289-295.
- [10] Hanson, A. R., Domich, E. G., and Adams, H. S., 1963, "Shock Tube Investigation of the Breakup of Drops by Air Blasts," *The Physics of Fluids*, 6(8), pp. 1070-1080.
- [11] Gelfand, B. E., Gubin, S. A., Kogarko, S. M., and Komar, S. P., 1973, "Singularities of the breakup of viscous liquid droplets in shock waves," *Journal of engineering physics*, 25(3), pp. 1140-1142.
- [12] Hsiang, L. P., and Faeth, G. M., 1995, "Drop deformation and breakup due to shock wave and steady disturbances," *International Journal of Multiphase Flow*, 21(4), pp. 545-560.
- [13] Hsiang, L. P., and Faeth, G. M., 1992, "Near-limit drop deformation and secondary breakup," *International Journal of Multiphase Flow*, 18(5), pp. 635-652.
- [14] Hsiang, L. P., and Faeth, G. M., 1993, "Drop properties after secondary breakup," *International Journal of Multiphase Flow*, 19(5), pp. 721-735.
- [15] Zhao, H., Liu, H. F., Xu, J. L., and Li, W. F., 2011, "Experimental study of drop size distribution in the bag breakup regime," *Industrial & Engineering Chemistry Research*, 50(16), pp. 9767-9773.
- [16] Zhao, H., Liu, H.-F., Cao, X.-K., Li, W.-F., and Xu, J.-L., 2011, "Breakup characteristics of liquid drops in bag regime by a continuous and uniform air jet flow," *International Journal of Multiphase Flow*, 37(5), pp. 530-534.
- [17] Zhao, H., Liu, H.-F., Xu, J.-L., Li, W.-F., and Lin, K.-F., 2013, "Temporal properties of secondary drop breakup in the bag-stamen breakup regime," *Physics of Fluids*, 25(5), p. 054102.
- [18] Han, J., and Tryggvason, G., 2001, "Secondary breakup of axisymmetric liquid drops. II. Impulsive acceleration," *Physics of Fluids*, 13(6), pp. 1554-1565.
- [19] Aalburg, C., 2002, Deformation and breakup of round drops and nonturbulent liquid jets in uniform crossflows.
- [20] Quan, S., and Schmidt, D. P., 2006, "Direct numerical study of a liquid droplet impulsively accelerated by gaseous flow," *Physics of Fluids (1994-present)*, 18(10), p. 102103.
- [21] Wadhwa, A. R., Magi, V., and Abraham, J., 2007, "Transient deformation and drag of decelerating drops in axisymmetric flows," *Physics of Fluids (1994-present)*, 19(11), p. 113301.

- [22] Jing, L., and Xu, X., 2010, "Direct Numerical Simulation of Secondary Breakup of Liquid Drops," *Chinese Journal of Aeronautics*, 23(2), pp. 153-161.
- [23] Kékesi, T., Amberg, G., and Prah Wittberg, L., 2014, "Drop deformation and breakup," *International Journal of Multiphase Flow*, 66, pp. 1-10.
- [24] Yang, W., Jia, M., Sun, K., and Wang, T., 2016, "Influence of density ratio on the secondary atomization of liquid droplets under highly unstable conditions," *Fuel*, 174, pp. 25-35.
- [25] Yang, W., Jia, M., Che, Z., Sun, K., and Wang, T., 2017, "Transitions of deformation to bag breakup and bag to bag-stamen breakup for droplets subjected to a continuous gas flow," *International Journal of Heat and Mass Transfer*, 111, pp. 884-894.
- [26] Shao, C., Luo, K., and Fan, J., 2017, "Detailed numerical simulation of unsteady drag coefficient of deformable droplet," *Chemical Engineering Journal*, 308, pp. 619-631.
- [27] Hirt, C. W., and Nichols, B. D., 1981, "Volume of fluid (VOF) method for the dynamics of free boundaries," *Journal of Computational Physics*, 39(1), pp. 201-225.
- [28] Lafaurie, B., Nardone, C., Scardovelli, R., Zaleski, S., and Zanetti, G., 1994, "Modelling Merging and Fragmentation in Multiphase Flows with SURFER," *Journal of Computational Physics*, 113(1), pp. 134-147.
- [29] Stefanitsis, D., Malgarinos, I., Strotos, G., Nikolopoulos, N., Kakaras, E., and Gavaises, M., "Numerical investigation of the aerodynamic breakup of Diesel droplets under various gas pressures," *Proc. ILASS-Europe 2017*.
- [30] Malgarinos, I., Nikolopoulos, N., and Gavaises, M., 2015, "Coupling a local adaptive grid refinement technique with an interface sharpening scheme for the simulation of two-phase flow and free-surface flows using VOF methodology," *Journal of Computational Physics*, 300, pp. 732-753.
- [31] Malgarinos, I., Nikolopoulos, N., Marengo, M., Antonini, C., and Gavaises, M., 2014, "VOF simulations of the contact angle dynamics during the drop spreading: Standard models and a new wetting force model," *Advances in Colloid and Interface Science*, 212, pp. 1-20.
- [32] Malgarinos, I., Nikolopoulos, N., and Gavaises, M., 2016, "A numerical study on droplet-particle collision dynamics," *International Journal of Heat and Fluid Flow*, 61, Part B, pp. 499-509.
- [33] Malgarinos, I., Nikolopoulos, N., and Gavaises, M., 2017, "Numerical investigation of heavy fuel droplet-particle collisions in the injection zone of a Fluid Catalytic Cracking reactor, Part I: Numerical model and 2D simulations," *Fuel Processing Technology*, 156, pp. 317-330.
- [34] Malgarinos, I., Nikolopoulos, N., and Gavaises, M., 2017, "Numerical investigation of heavy fuel droplet-particle collisions in the injection zone of a Fluid Catalytic Cracking reactor, part II: 3D simulations," *Fuel Processing Technology*, 156, pp. 43-53.
- [35] G. Strotos, I. M., N. Nikolopoulos, K. Papadopoulos, A. Theodorakakos, M. Gavaises, 2015, "Performance of VOF methodology in predicting the deformation and breakup of impulsively accelerated droplets," *ICLASS 2015, 13th Triennial International Conference on Liquid Atomization and Spray Systems, August 23-27 Tainan, Taiwan*.
- [36] Strotos, G., Malgarinos, I., Nikolopoulos, N., and Gavaises, M., 2016, "Predicting droplet deformation and breakup for moderate Weber numbers," *International Journal of Multiphase Flow*, 85, pp. 96-109.
- [37] Strotos, G., Malgarinos, I., Nikolopoulos, N., and Gavaises, M., 2016, "Aerodynamic breakup of an n-decane droplet in a high temperature gas environment," *Fuel*, 185, pp. 370-380.
- [38] Strotos, G., Malgarinos, I., Nikolopoulos, N., and Gavaises, M., 2016, "Numerical investigation of aerodynamic droplet breakup in a high temperature gas environment," *Fuel*, 181, pp. 450-462.
- [39] Strotos, G., Malgarinos, I., Nikolopoulos, N., and Gavaises, M., 2016, "Predicting the evaporation rate of stationary droplets with the VOF methodology for a wide range of ambient temperature conditions," *International Journal of Thermal Sciences*, 109, pp. 253-262.
- [40] Kolev, N. I., 2012, "Diesel fuel properties," *Multiphase Flow Dynamics 4*, Springer Berlin Heidelberg.
- [41] Kyriakides, N., Chryssakis, C., and Kaiktsis, L., 2009, "Influence of Heavy Fuel Properties on Spray Atomization for Marine Diesel Engine Applications," *SAE International*.
- [42] Clift, R., Grace, J. R., and Weber, M. E., 2005, *Bubbles, drops, and particles*, Courier Corporation.
- [43] Jalaal, M., and Mehravaran, K., 2014, "Transient growth of droplet instabilities in a stream," *Physics of Fluids*, 26(1), p. 012101.
- [44] Khare P., V. Y., "Drag Coefficients of Deforming and Fragmenting Liquid Droplets," *Proc. ILASS Americas, 25th Annual Conference on Liquid Atomization and Spray Systems*.
- [45] Pilch, M., and Erdman, C. A., 1987, "Use of breakup time data and velocity history data to predict the maximum size of stable fragments for acceleration-induced breakup of a liquid drop," *International Journal of Multiphase Flow*, 13(6), pp. 741-757.
- [46] Dai, Z., and Faeth, G. M., 2001, "Temporal properties of secondary drop breakup in the multimode breakup regime," *International Journal of Multiphase Flow*, 27(2), pp. 217-236.
- [47] Kiya, M., Ishikawa, H., and Sakamoto, H., 2001, "Near-wake instabilities and vortex structures of three-dimensional bluff bodies: a review," *Journal of Wind Engineering and Industrial Aerodynamics*, 89(14-15), pp. 1219-1232.
- [48] Sakamoto, H., and Haniu, H., "A study on vortex shedding from spheres in a uniform flow."
- [49] Achenbach, E., 1974, "Vortex shedding from spheres," *Journal of Fluid Mechanics*, 62(02), pp. 209-221.
- [50] Hirahara, H., and Kawahashi, M., 1992, "Experimental investigation of viscous effects upon a breakup of droplets in high-speed air flow," *Experiments in Fluids*, 13(6), pp. 423-428.
- [51] Yaws, C. L., "Yaws' Handbook of Thermodynamic Properties for Hydrocarbons and Chemicals," Knovel.
- [52] Yaws, C. L., 2009, "Chapter 7 - Thermal Conductivity of Liquid – Organic Compounds," *Transport Properties of Chemicals and Hydrocarbons*, William Andrew Publishing, Boston, pp. 299-395.

